Published in final edited form as:
Phys Rev E Stat Nonlin Soft Matter Phys. 2009 June ; 79(6 Pt 1): 061924. doi:10.1103/PhysRevE.79.061924.

Nonlinear phase interaction between nonstationary signals: A comparison study of methods based on Hilbert-Huang and Fourier transforms

Men-Tzung Lo[1,2,3,†], **Vera Novak**[1], **C.-K. Peng**[2], **Yanhui Liu**[4], and **Kun Hu**[1,5,‡]

[1] Division of Gerontology, Beth Israel Deaconess Medical Center, Harvard Medical School, Boston, Massachusetts 02215, USA

[2] Division of Interdisciplinary Medicine and Biotechnology and Margret and H. A. Rey Institute for Nonlinear Dynamics in Medicine, Beth Israel Deaconess Medical Center, Harvard Medical School, Boston, Massachusetts 02215, USA

[3] Research Center for Adaptive Data Analysis, National Central University, Chungli 32054, Taiwan, Republic of China

[4] DynaDx Corporation, Mountain View, California 94041, USA

[5] Division of Sleep Medicine, Brigham and Women's Hospital, Harvard Medical School, Boston, Massachusetts 02215, USA

Abstract

Phase interactions among signals of physical and physiological systems can provide useful information about the underlying control mechanisms of the systems. Physical and biological recordings are often noisy and exhibit nonstationarities that can affect the estimation of phase interactions. We systematically studied effects of nonstationarities on two phase analyses including (i) the widely used transfer function analysis (TFA) that is based on Fourier decomposition and (ii) the recently proposed multimodal pressure flow (MMPF) analysis that is based on Hilbert-Huang transform (HHT) —an advanced nonlinear decomposition algorithm. We considered three types of nonstationarities that are often presented in physical and physiological signals: (i) missing segments of data, (ii) linear and step-function trends embedded in data, and (iii) multiple chaotic oscillatory components at different frequencies in data. By generating two coupled oscillatory signals with an assigned phase shift, we quantify the change in the estimated phase shift after imposing artificial nonstationarities into the oscillatory signals. We found that all three types of nonstationarities affect the performances of the Fourier-based and the HHT-based phase analyses, introducing bias and random errors in the estimation of the phase shift between two oscillatory signals. We also provided examples of nonstationarities in real physiological data (cerebral blood flow and blood pressure) and showed how nonstationarities can complicate result interpretation. Furthermore, we propose certain strategies that can be implemented in the TFA and the MMPF methods to reduce the effects of nonstationarities, thus improving the performances of the two methods.

Correspondence to: Men-Tzung Lo; Kun Hu.
[†]FAX: +886-3-426-9734; d88942007@ntu.edu.tw
[‡]FAX: 617-667-0351; khu@bidmc.harvard.edu

PACS number(s): 87.85.Ng, 87.85.Xd, 87.50.sg

I. INTRODUCTION

Many physical and physiological systems possess multiple feedback interactions among system components or control nodes [1,2]. Phase relationship among output signals of these systems can provide insights into underlying control mechanisms of these interactions [3–5]. Traditional approaches to quantify phase relationship are based on Fourier transform, which assumes stationary signals consisting of sinusoidal wave forms. However, due to nonlinear coupling among multiple interactions, signals of complex systems are typically nonstationary [statistical properties such as mean and standard deviation (SD) vary with time] [6–8]. Thus, Fourier-based approaches are believed to be unreliable for the analysis of nonstationary signals.

To resolve the difficulties related to nonstationarity, Hilbert-Huang transform (HHT) that is based on nonlinear chaotic theories has been designed to extract dynamic information from nonstationary signals at different time scales [9]. In the last 10 years, the HHT has been utilized in more than 2000 published works and has been applied in a various of research fields such as climate research [10–12], orbit research [13], structural health monitoring [14–17], water wave analysis [18,19], blood pressure hemodynamics [20], cerebral autoregulation [21–23], cardiac dynamics [24], respiratory dynamics [25], and electroencephalographic activity [26]. Recently, the HHT has been applied to quantify nonlinear phase interaction between nonstationary signals [21–23]. The HHT-based phase analysis, namely, multimodal pressure flow (MMPF), does not assume stationarity and is thus believed to be more reliable than traditional Fourier-based methods [22,27]. However, no systematic studies have been conducted to compare the performance of the MMPF method with those of traditional approaches, especially for the assessment of phase interactions between nonstationary signals.

Here we systematically study the performance of the HHT-based MMPF method using two oscillatory signals with prior known phase relationship. We also compare the MMPF with the transfer function analysis (TFA), a Fourier-based method that has been widely used to quantify phase relationship between two coupled signals in many physical and physiological systems such as complex structures and viscoelastic materials [28], seismological monitoring system [29], and cardiovascular control systems [30–33]. We examine the effects on the two methods of three different types of nonstationarities that are often observed in real-world recordings:

(1) Missing segments of data

During continuous signal recordings, it is often to have portions of data that are unreliable and therefore need to be discarded, e.g., blood pressure monitor often calibrates every 1 min in order to compensate for or correct the possible baseline drift. The missing data are usually replaced with interpolated values obtained from local fitting or by the global mean value. Recognizing effects of such procedure on phase analyses is important for correct result interpretations.

(2) Linear and step-function trends

The existence of trends in physical and physiological time series is so common that it is almost unavoidable. For instances, an increased resistance due to an increased temperature in an electronic circuit can lead to a decrease in electric current, the ocean temperature drops after the sun set and changes at different depth levels, the heart rate can increase quickly due to mental stress, and the blood flow velocity can drop suddenly due to respiration-related CO_2 changes. Mathematically, these gradual and sharp changes can be approximately described by linear and step functions, respectively. Here we study trends of two simple forms (i.e., linear and step functions) and examine their effects on the estimations of phase interactions between two oscillators. We consider the cases when trends are independent of the mechanisms related to or controlling the phase interactions between two oscillators.

(3) Mixed chaotic oscillations at different frequencies

A physical or physiological system usually contains many control nodes that influence the system at different frequencies. Thus, signals of the system may have multiple oscillatory components centered at different frequencies, and each component may represent a distinct underlying mechanism. Additionally, each oscillatory component in each signal is not necessarily stationary with sinusoidal wave forms but rather displays a chaotic behavior as characterized by a broad peak in power spectrum (i.e., the amplitude and period of an oscillator vary at different times). Therefore, it is often difficult or even impossible to separate different components based on Fourier transform. To determine effects of nonstationarity associated with multiple oscillatory components and their varying wave forms on phase analysis, we consider the cases that two signals have two corresponding oscillatory components and the phase interaction between two signals is different when choosing different corresponding components (see details in Sec. II A 2).

To test and compare performances of the MMPF and the TFA, we generate two oscillatory signals with an assigned constant phase shift. We generate the first oscillatory signal using sinusoidal wave forms, and the other signal using the same instantaneous amplitudes and phases of the first signal but with an assigned phase shift (see details in Sec. II A). For such two stationary oscillations, the MMPF and the TFA should give the same phase relationship, i.e., a constant phase shift between two signals that is equal to the assigned phase shift. Next we will artificially introduce nonstationarities into the signals and perform the MMPF and the TFA methods on the nonstationary signals (Sec. II A). Deviations of the new phase shifts from the originally assigned phase shift value will reveal influences of nonstationarities on the two methods. We note that a real physical or physiological time series often possesses different types of nonstationarities at different time windows (Sec. IV and Appendix C). In order to understand the superposed effects of all nonstationarities in real data on phase analysis, it is important to use the deductive approach to understand effects of each type of nonstationarities, separately.

The layout of the paper is as follows. In Sec. II, we briefly introduce the TFA and the MMPF methods. We also describe how to generate two signals with designed phase relationship and how to introduce different types of nonstationarities. In Sec. III, we present our simulation results and demonstrate effects of nonstationarities caused by missing data, linear trends, step functions, and mixed oscillatory modulations at different frequencies. We also compare the performances of the MMPF and the TFA and discuss certain strategies to minimize effects of nonstationarities on the two methods. In Sec. IV, we provide examples of nonstationarities and their effects on the MMPF and the TFA in real physiological data analysis (cerebral blood flow velocity and blood pressure). Data was collected from the previous studies that were in accordance with the Helsinki Declaration of the World Medical Associations and were approved by the institutional human subjects Internal Review Board at Beth Israel Deaconess Medical Center. All subjects provided written informed consent prior to participation. In Sec. V, we summarize our results and discuss the advantages and the disadvantages of the two methods.

II. METHODS

A. Surrogate signals

To test performances of the MMPF and the TFA, we generate two oscillatory signals denoted as $I(t)$ and $O(t)$ that have assigned phase interactions. For convenience, we call $I(t)$ the input signal and $O(t)$ the output signal. To simplify the interpretation of the simulation results, two signals have oscillations centered at the frequency f_0 and with an assigned constant phase shift

$\Delta\theta(t) = \Delta\theta_0 = \pi/10 = 18°$. The length of the signal is 5 min, and the sampling frequency of each signal is 50 Hz ($t = 0.02i$, $i = 0,1,2,3, \ldots, 15\,000$).

1. Surrogate signals with missing data or trends—To simulate signals with nonstationarities caused by *missing segments of data* and trends, we generate $I(t)$ and $O(t)$ in the following steps:

Step 1: First, we generate a stationary oscillatory signals that have sinusoidal wave forms with a constant amplitude and frequency: $I_0(t) = A_0 \cos(2\pi f_0 t)$.

Step 2: The Hilbert transform of $I_0(t)$ is obtained by

$$\tilde{I}_0(t) = \frac{1}{\pi} P \int \frac{I_0(t')}{t - t'} dt', \tag{1}$$

where P denotes the Cauchy principal value. The instantaneous amplitude $A_I(t)$ and the phase $p_I(t)$ of $I_0(t)$ can be calculated from the analytical signal as follows:

$$I_0(t) + i\tilde{I}_0(t) = A_I(t) e^{jp_I(t)} \tag{2}$$

For the sinusoidal function, $A_I(t) = A_0$ and $p_I(t) = 2\pi f_0 t$.

Step 3: We generate the second signal $O(t)$ by adding a phase shift $\Delta\theta(t)$ to $p_I(t)$ while keeping the same instantaneous amplitude $A_I(t)$,

$$O(t) = \mathrm{Re}[A_I(t) e^{j[p_I(t) + \Delta\theta(t)]}] = A_I(t) \cos[p_I(t) + \Delta\theta(t)]. \tag{3}$$

Here we consider two signals with a constant phase lag $\Delta\theta(t) = \Delta\theta_0$. Thus,

$$O(t) = A_I(t) \cos[p_I(t) + \Delta\theta_0]. \tag{4}$$

For the sinusoidal wave form $I_0(t) = A_0 \cos(2\pi f_0 t)$, $O(t) = A_0 \cos(2\pi f_0 t + \Delta\theta_0)$.

Step 4: (1) To test the effect of nonstationarity associated with missing segments of data, we divide $O_0(t)$ into nonoverlapped 10-s segments, randomly chose *m%* of all segment, and replace points in the chosen segments with the global mean. (2) To test the effect of nonstationarity associated with trends, we superpose $O_0(t)$ with a linear trend $y(t) = a_0 + b_0 t$ or a step-function trend $y(t) = \begin{cases} 0 & t < t_1 \\ G & t \geq t_1 \end{cases}$, where a_0, b_0, and G are constants: $O(t) = O_0(t) + y(t)$.

2. Surrogate signals with mixed chaotic oscillations at different frequencies—To simulate more realistic and more complex nonstationarities, we generate two oscillatory signals with varying frequency and amplitude. Additionally, we introduce to each signal a second oscillatory component that is independent of the original oscillation component but may have a Fourier spectrum with overlaps (frequent band) with the original component. We consider the case that the phase relationship between the additional components in the input

and the output signals is different from that between the first components. For simplicity, we assign the phase lag zero for the additional oscillatory components in two signals. The procedure includes the following steps:

Step 1: We generate a set of one cycle sinusoidal wavelets [i.e., $\phi_i(t)=A_i\cos(2\pi\frac{t}{T_i})$, $0\le t\le T_i$], where the amplitude A_i and the period T_i obey uniform distributions. The mean and the standard deviation are $\langle A\rangle$ and δ_A for A_i, and $\bar{T}=1/f_0$ and δ_T for T_i, respectively.

Step 2: Next we construct a nonstationary signal $I_0(t)$ by stitching these sinusoidal wavelets together.

Step 3: We generate $O_0(t)$ from $I_0(t)$ in the same way as described in Sec II A 1 (steps 2 and 3) for pure sinusoidal $I_0(t)$.

Step 4: We repeat steps 1–3 to generate a second pair of oscillatory signals, $I_1(t)$ and $O_1(t)$, by choosing a different set of periods T_i' with a different mean period $\bar{T}'$ or frequency $\bar{f}'=1/\bar{T}'$. In addition, we assign the phase shift 0 for the two new oscillators.

Step 5: We superpose $I_0(t)$ with $I_1(t)$ to generate $I(t)=I_0(t)+\lambda I_1(t)$, and $O_0(t)$ with $O_1(t)$ to generate $O(t)=O_0(t)+\lambda O_1(t)$, where λ is the weight of the second oscillatory component in each signal.

The generated $I(t)$ and $O(t)$ have two mixed chaotic oscillations centered at different frequencies and the phase lag between two signals at the two frequencies are different [$\Delta\theta_0=\pi/10$ between $I_0(t)$ and $O_0(t)$, and 0 between $I_1(t)$ and $O_1(t)$].

B. Transfer function analysis

The TFA is based on Fourier transform. The main concept of the method is to decompose each signal into multiple sinusoidal wave forms at different frequencies and to compare the amplitudes and phases of components between two signals at each frequency. To illustrate the TFA algorithm, we consider an input signal $I(t)$ and an output signal $O(t)$, each with 5 min and a sampling rate of 50 Hz (15 000 data points). The two time series are first divided into 100-s segments with 50% overlap (i.e., each segment). In each segment, the Fourier transform of $I(t)$, denoted as $S_I(f)$, and the Fourier transform of $O(t)$, denoted as $S_O(f)$, are calculated with a spectral resolution of 0.02 Hz. Then $S_I(f)$ and $S_O(f)$ were used to calculate the transfer function

$$H(f)=\frac{S_I(f)S_O^*(f)}{|S_I(f)|^2}=G(f)e^{j\varphi(f)}, \tag{5}$$

where $S_O^*(f)$ is the conjugate of $S_O(f)$, $|S_I(f)|^2$ is the power spectrum density of $I(t)$, $G(f)=|H(f)|$ is the transfer function amplitude (gain), and $\varphi(f)$ is the transfer function phase at frequency f. Then the average G and φ are obtained within an interested frequency band (e.g., 0.3±0.02 Hz for the simulated 0.3 Hz oscillator and 0.75±0.02 Hz for 0.75 Hz oscillator in this study) from all segments. For two oscillatory signals with a constant period and with a fixed phase shift, e.g., $I(t)=A_0\cos(2\pi f_0 t)$ and $O(t)=A_0\cos(2\pi f_0 t+\Delta\theta_0)$, the average transfer function phase at $f=f_0$ is $\Delta\theta_{\mathrm{TFA}}\equiv\bar{\varphi}=\Delta\theta_0$.

In addition to the assumption that signals are composed of sinusoidal wave forms, transfer function analysis also assumes the linear relationship between two signals. Thus, the method

calculates a parameter, called *coherence*, to indicate whether the assumed linear relationship is reliable. The coherence $C(f)$ is defined by

$$C(f)=\frac{|S_I(f)S_O^*(f)|^2}{|S_I(f)|^2|S_O(f)|^2}. \tag{6}$$

Ranging from 0 to 1, the coherence value close to 0 indicates the lack of linear relationship between the input and the output signals. Therefore, $G(f)$ and $\varphi(f)$ cannot be used if $C(f)$ is too small (<0.5).

C. Multimodal pressure-flow method

The MMPF method includes four major steps: (1) decomposition of each signal (the input and the output) into multiple empirical modes, (2) selection of empirical modes for (dominant) oscillations in the input signal and corresponding oscillations in the output signal, (3) calculation of instantaneous phases of the extracted input and output oscillations, and (4) calculation of input-output phase relationship.

Step 1—Empirical mode decomposition. To achieve the first major step of MMPF, empirical mode decomposition (EMD) algorithm based on Hilbert-Huang transform is used to decompose each signal into multiple empirical modes, called intrinsic mode functions (IMFs) [20]. Each IMF represents a frequency-amplitude modulation in a narrow band that can be related to a specific physical or physiologic process [20].

For a time series $x(t)$ with at least two extremes, the EMD extracts IMFs one by one from the smallest scale to the largest scale using a sifting procedure

$$\begin{aligned} x(t)&=c_1(t)+r_1(t)\\ &=c_1(t)+c_2(t)+r_2(t)\\ &\vdots\\ &=c_1(t)+c_2(t)+\cdots+c_n(t), \end{aligned} \tag{7}$$

Where $c_k(t)$ is the kth IMF component and $r_k(t)$ is the residual after extracting the first k IMF components [i.e., $r_k(t)=x(t)-\sum_{i=1}^{k}c_i(t)$]. Briefly, the extraction of the kth IMF includes the following steps:

- **i.** Initialize $h_0(t)=h_{i-1}(t)=r_{k-1}(t)$ [if k=1, $h_0(t)=x(t)$], where i=1.
- **ii.** Extract local minima and maxima of $h_{i-1}(t)$ [if the total number of minima and maxima is less than 2, $c_k(t)=h_{i-1}(t)$ and stop the whole EMD process].
- **iii.** Obtain upper envelope (from maxima) and lower envelope (from minima) functions $p(t)$ and $v(t)$ by interpolating local minima and maxima of $h_{i-1}(t)$, respectively.
- **iv.** Calculate $h_i(t)=h_{i-1}(t)-\frac{p(t)+v(t)}{2}$.
- **v.** Calculate the SD of $\frac{p(t)+v(t)}{2}$.
- **vi.** If SD is small enough (less than a chosen threshold SD max, typically between 0.2 and 0.3) [20], the kth IMF component is assigned as $c_k(t)=h_i(t)$ and $r_k(t)=r_{k-1}(t)-c_k(t)$; otherwise, repeat steps (ii)–(v) for i+1 until SD < SD max.

Steps (i)–(vi) are repeated to obtain different IMFs at different scales until there are less than two minima or maxima in a residual $r_{k-1}(t)$, which will be assigned as the last IMF [see the step (ii) above] (Fig. 1).

To better extract oscillations embedded in nonstationary physiology signals, a noise assisted EMD, called ensemble EMD (EEMD) [34], has been implemented in the MMPF method (see details in Appendix A). The EEMD technique can ensure that each component does not consist of oscillations at dramatically disparate scales, and different components are locally nonoverlapping in the frequency domain. Thus, each component obtained from the EEMD may better represent fluctuations corresponding to a specific physical and physiologic process.

Step 2—Mode selection. The second step of the MMPF is to choose an IMF for the input signal $I(t)$ and the corresponding IMF for the output signal $O(t)$. How to select an IMF depends on the interested frequency range under study. Here we focus on in the frequency band centered at a given frequency f_0. The selected IMFs denoted by $\hat{I}(t)$ and $\hat{O}(t)$ are used for the analysis of phase relationship.

Step 3—Instantaneous phases of oscillators. The third step of the MMPF analysis is to obtain instantaneous phases of two oscillations using Hilbert transform (see Sec. II A 1). For the chosen IMFs, $\hat{I}(t)$ and $\hat{O}(t)$, we use Eqs. (1) and (2) to obtain their instantaneous phases, $p_I(t)$ and $p_o(t)$, respectively.

Step 4—Phase relationship between two oscillations. The instantaneous phase shift between two oscillators can be calculated as $\Delta\theta(t) = p_o(t) - p_I(t)$. There are many indices that can be derived from the phase shift time series $p_I(t)$ and $p_o(t)$ [or $\Delta\theta(t)$] to characterize phase relationship between the two oscillators, including the mean and the standard deviation of phase shifts [21–23], and synchronization index [5,35] and cross-correlation index [36]. In this study, since we consider two oscillatory signals with a preassigned constant phase shift, we use the mean phase shift in each simulation $\Delta\theta_{\mathrm{MMPF}} = \overline{\Delta\theta(t)}$ to quantify the phase relationship.

III. SIMULATION RESULTS

A. Effects of missing data

In this section, we study how missing data affect the performances of the MMPF and the TFA. We artificially introduce missing data in the output signal $O(t) = A_0 \cos(2\pi f_0 t + \Delta\theta_0)$ by selecting a number of 10-s segments and replacing the data points in the segments with the global mean (zeros in the simulations) [Fig. 2(b)]. For simplicity, the input signal $I_0(t) = A_0 \cos(2\pi f_0 t)$ has no missing data [Fig. 2(a)]. Because the signal length is 300 s, each missing segment corresponds to 3.33% of the total data points. For a given number of missing segments or a given percentage of missing data, we repeat the simulation 50 times, each time with randomly selected 10-s segments. In each simulation, we perform the MMPF and the TFA analyses to obtain $\Delta\theta_{\mathrm{MMPF}}$ and $\Delta\theta_{\mathrm{TFA}}$.

The results indicate that (i) the MMPF underestimates the phase shift between two signals due to missing data ($\Delta\theta_{\mathrm{MMPF}} < \Delta\theta_0$) [Fig. 2(b)] and (ii) the difference between $\Delta\theta_{\mathrm{MMPF}}$ and $\Delta\theta_0$ (i.e., $\Delta\theta_{\mathrm{MMPF}} - \Delta\theta_0$) is linearly proportional to the percentage of missing data [Fig. 3(a)]. To explore the underlying reason for the effect of missing data, we study the instantaneous phase shift $\Delta\theta(t)$ between selected IMFs of $I(t)$ and $O(t)$. We observe that $\Delta\theta(t)$ in the missing segments displays large fluctuations with values approximately distributing uniformly from $-\pi$ to π ($-180°$ to $180°$) [Fig. 3(b)]. Clearly, these artifacts caused by missing oscillatory cycles in $O(t)$ induce a white noise background in $\Delta\theta(t)$ and the average of these artifact values is

zero. Since $\Delta\theta_{\mathrm{MMPF}}$ is the average of all points in $\Delta\theta(t)$ including $m\%$ data for missing segments, we can obtain

$$\Delta\theta_{\mathrm{MMPF}}=(m/100)\times 0+(1-m/100)\Delta\theta_0=\Delta\theta_0-\frac{\Delta\theta_0}{100}m. \tag{8}$$

The derived analytical relationship between $\Delta\theta_{\mathrm{MMPF}}$ and the percentage of missing data (m) is consistent with the simulation results. With the knowledge of how missing data affect $\Delta\theta(t)$, we can improve the performance of the MMPF by (i) calculating the median of $\Delta\theta(t)$, (ii) removing a uniform (white-noise) background in the distribution of $\Delta\theta(t)$ and calculating $\Delta\theta_{\mathrm{MMPF}}$ as the average of the remain values, or (iii) identifying and removing artifact data points in those cycles with huge jumps (to 180°) and drops (to −180°). Using the second strategy (see Appendix B), the improved MMPF essentially eliminates the effect of missing data, yielding a phase shift $\Delta\theta_{\mathrm{MMPF}}$ that is identical to $\Delta\theta_0$ [Fig. 2(b)].

For the TFA, we found that the average of $\Delta\theta_{\mathrm{TFA}}$ obtained from 50 simulations is close to (or not significantly different from) $\Delta\theta_0$. However, there is a large variation in the values obtained in different realizations, as indicated by the large standard deviation of $\Delta\theta_{\mathrm{TFA}}$ values [Fig. 2(b)]. The variation becomes larger when the oscillation frequency is lower (smaller f_0 =0.3 Hz) [Fig. 2(c)]. Although it is clear that the random error is caused by the altered Fourier transform due to missing data, there is no efficient way to compensate for such an influence in each simulation. The realistic approach that can minimize the effect on the TFA is to select signals without missing data or to rely on a large number of simulations in order to obtain a more reliable average.

B. Effect of linear trend

In this section, we consider the case in which the input signal $I(t)$ is a pure sinusoidal signal $I_0(t)=A_0\cos(2\pi f_0 t)$ and the output signal is a sinusoidal signal $O_0(t)=A_0\cos(2\pi f_0 t+\Delta\theta_0)$ with a linear trend $y(t)=a_0+b_0 t$ [Fig. 4(a)]. We apply the MMPF to $I(t)$ and $O(t)$. The decomposition procedure of the MMPF (EMD or EEMD) can perfectly separate and the linear trend (IMF in mode 1) and the sinusoidal component (IMF in mode 2) in the output signal [Fig. 4(b)]. Thus, the phase difference between the input and the output signals obtained from the MMPF at the given frequency f_0 is identical to the assigned value $\Delta\theta_{\mathrm{MMPF}}=\Delta\theta_0=18°$. The result remains the same for different frequencies f_0 of the sinusoidal signal and different slopes b_0 of the linear trend [Fig. 4(d)]. We also apply the TFA on the same $I(t)$ and $O(t)$. The transfer phase angle is $\Delta\theta_{\mathrm{TFA}}=18°$ when $b_0=0$ (i.e., no linear trend). However, when $b_0>0$, $\Delta\theta_{\mathrm{TFA}}$ deviates from the expected value and becomes larger and larger for increasing b_0 [Fig. 4(d)]. The increase in $\Delta\theta_{\mathrm{TFA}}$ is more pronounced for the sinusoidal wave form with a lower frequency (smaller f_0), e.g., the deviation is larger for f_0 =0.3 Hz compared to f_0 =0.75 Hz [Fig. 4(d)].

The effect of the linear trend on the TFA can be easily understood when considering the Fourier transform of the linear trend [Fig. 4(c)]. Due to the assumption of sinusoidal wave forms in the Fourier transform, the linear trend has a significant contribution to all frequency bands in Fourier space, especially to the lower-frequency band (smaller f_0) [Fig. 4(c)], thus affecting the oscillatory component centered at f_0. The overestimation of the phase shift with the presence of a linear trend is caused by the fact that the Fourier phase of a linear trend is between 90° and 180° [Fig. 4(c)], which is much greater than the assigned phase shift $\Delta\theta_0=18°$ between two oscillations. Therefore, to minimize effects of the linear trend and to obtain reliable estimate of phase shift between two oscillatory signals, a detrending process (i.e., removing polynomial trends in two signals) is usually performed before applying the TFA method [32]. It is a general misunderstanding that polynomial fit can efficiently remove trends, so that the

identified effect of linear trends on phase analysis is not a serious concern. On the contrary, filtering trends is not a trivial task because different local trends can be present at different time windows in real signals [37]. As we demonstrated in Appendix C, detrending by polynomial fit can lead to residual trend that may still complicate phase analysis.

C. Effect of step function

In this section, we study the influence of sudden drift in the recording on the MMPF and the TFA methods. The sudden drift is modeled mathematically as a step function,

$$y(t)=\begin{cases} 0 & t<t_1 \\ G & t \geq t_1, \end{cases} \tag{9}$$

where G is a constant and t_1 is randomly chosen from a uniformly distributed values from 0–300 s. Thus, we consider the input signal $I(t) = A_0 \cos(2\pi f_0 t)$ and the output signal $O(t) = A_0 \cos(2\pi f_0 t + \Delta\theta_0) + y(t)$ [Fig. 5(c)].

For the MMPF method, a step function contributes to different components or IMFs at different frequency bands [Fig. 5(b)]. Thus, the step function in the input signal affects the extracted oscillatory component of at frequency f_0, leading to a certain deviation of the phase shift $\Delta\theta_{\mathrm{MMPF}}$ from the expected value $\Delta\theta_0 = 18°$ [Fig. 5(e)]. The contribution of the step function to each IMF displays a similar wave form shape although the scale of the wave form is different for different IMFs. It is important to note that the influence of step function on each IMPF is localized and centered at $t = t_1$. Thus, the step function affects the instantaneous phase shift $\Delta\theta(t)$ mainly at $\sim t_1$. [Fig. 5(c)]. We can minimize the effect of the step function on the MMPF in the same way as in the case of missing data, i.e., filtering out the outlines in instantaneous phase shift $\Delta\theta(t)$ (Appendix B).

A step function also affects the performance of the TFA, leading to (1) an overestimation of the mean phase shift ($\Delta\theta_{\mathrm{TFA}} > \Delta\theta_0$) and (2) a variation in $\Delta\theta_{\mathrm{TFA}}$ in different realizations [Fig. 5(e)]. The effect of step function is much stronger for low-frequent oscillatory signals compared to high-frequent signals, i.e., $\Delta\theta_{\mathrm{TFA}}$ increases more for lower frequency f_0 [Fig. 5(e)]. Similar to the case with a linear trend, the frequency-dependent effect of a step function is due to that the Fourier amplitude of a step function is averagely larger in lower-frequency band than in higher-frequency band [Fig. 5(d)]. However, unlike a linear trend, the Fourier amplitude of a step function displays “notches” at certain specific frequencies where Fourier amplitude becomes zero [Fig. 5(d)]. Theoretically, if f_0 in our simulation is the frequency corresponding to certain notch and the mean phase shift $\Delta\theta_{\mathrm{TFA}}$ is obtained at the same frequency point, $\Delta\theta_{\mathrm{TFA}}$ should be the same as $\Delta\theta_0 = 18°$ (no effect from the step function). However, this case can hardly occur in a real study because the frequencies of the input and the output signals unlikely coincide with the notch frequency of a step function and the TFA phase shift is always based on the average results in a preselected frequency band.

D. Mixed nonstationary oscillations at different frequencies

In this section, we consider input signals $I(t) = I_0(t) + \lambda I_1(t)$ with two oscillation components, i.e., an additional oscillator $I_1(t)$ is embedded in the original oscillatory signal $I_0(t)$. To better mimic real nonstationary physical and physiological signals, we create each oscillation component [$I_0(t)$ and $I_1(t)$] that has varying amplitude and period [Figs. 6(a)–6(c)]. The output signal $O(t) = O_0(t) + \lambda O_1(t)$ has also two corresponding components: one component $O_0(t)$ has the same instantaneous amplitude as $I_0(t)$ but has a constant phase advance $\Delta\theta_0 = 18°$, and $O_1(t)$ is the same as $I_0'(t)$ (see Sec. II A 2 for details).

First we consider that the oscillation periods of the two components in $I(t)$ have no overlapping [Fig. 6(e)]: (i) the oscillation period of the interested component $I_0(t)$ has a uniform distribution from 3 to 4.2 s with the average $\bar{T}=1/f_0$ =3.6 s and (ii) the period of $I_1(t)$ has a uniform distribution from 1.2 to 1.8 with the average period of $\bar{T}' = 1/\bar{f}'$ =1.5 s. For a chosen weight λ of the second component [$I_1(t)$ and $O_1(t)$], we repeated the simulation 50 times. In each realization, amplitude, period, and order of oscillations in $I_0(t)$ and $I_1(t)$ are randomly generated. Generally, the MMPF can separate the two oscillatory components (modes 3 and 2 in Fig. 6 (d)], so that $\Delta\theta_{MMPF}$ is very close to the assigned phase difference between $I_0(t)$ and $O_0(t)$ ($\Delta\theta_0$ =18°) [Fig. 6(f)]. Increasing the weight of $I_1(t)$ does not significantly affect the mean value of $\Delta\theta_{MMPF}$ averaged over 50 realizations. However, $I_1(t)$ does induce certain random variation in different realizations, as characterized by a standard deviation of $\Delta\theta_{MMPF}$ that increases when the weight of $I_1(t)$, λ, increases [Fig. 6(d)]. In contrast to the MMPF, the TFA significantly underestimates the phase difference between $I_0(t)$ and $O_0(t)$ in the presence of the second oscillatory component $I_1(t)$. The deviation of $\Delta\theta_{TFA}$ from $\Delta\theta_0$ =18° increases with increasing the weight of $I_1(t)$. The influence on the TFA of the second oscillatory component is caused by the fact that $I_1(t)$ still has a slight contribution to the frequent band that is chosen to calculate transfer phase (0.25–0.3 Hz) [Fig. 6(e)]. This observation has an important implication for phase analysis of nonstationary signals, indicating that interested oscillatory components must be dominant in signals with multiple components for a reliable estimation of phase relationship by the TFA. In addition, there is a large variation in $\Delta\theta_{TFA}$ among different realizations even in the absence of the second oscillatory component (λ=0) [Fig. 6 (e)], indicating that nonstationarity associated with varying amplitude and cycle period can also affect the performance of the TFA. We further consider the case that the oscillation periods of the two components in $I(t)$ have certain overlap (Fig. 7): (i) the oscillation period of the interested component $I_0(t)$ has a uniform distribution from 3 to 6 s [Fig. 7(b)] and (ii) the period of $I_1(t)$ has a uniform distribution from 0.6 to 3.6 s [Fig. 7(c)]. Thus, the power spectra of two components have a significant overlapped part between 0.1 and 0.4 Hz [Fig. 7(e)]. Clearly, the MMPF cannot separate $I_0(t)$ and $I_1(t)$ very well, and the selected IMF that resembles $I_0(t)$ mostly [mode 4 in Fig. 7(d)] is also contributed partially from $I_1(t)$. As a result, the MMPF cannot estimate the phase shift between $I_0(t)$ and $O_0(t)$ very reliably ($\Delta\theta_{MMPF}<\Delta\theta_0$), and the deviation of $\Delta\theta_{MMPF}$ significantly increases when the weight of $I_1(t)$ increases [Fig. 7(e)]. For the TFA analysis, $\Delta\theta_{TFA}$ calculated at the frequency between 0.17 and 0.33 Hz is even smaller than $\Delta\theta_{MMPF}$ (i.e., deviating more away from the expected value $\Delta\theta_0$ =18°) [Fig. 7(f)]. This observation indicates that the second oscillation significantly affects the performances of the MMPF and TFA. This may be not surprising because the two corresponding components in $I(t)$ and $O(t)$ can have undistinguishable oscillations over a range of overlapped frequency and no existing empirical analysis can reliably separate these two components.

For signals with two oscillatory components, the above simulation results indicate that the MMPF performs relatively better than the TFA due to the fact that the EMD or the EEMD can better separate two oscillatory components than Fourier transform. With such a consideration, we propose to apply the TFA to the IMFs extracted from the EMD or the EEMD rather than to original signals. By applying the modified TFA to the same surrogate data, we showed that the estimated phase shift is much closer to the expected value, compared to the original TFA results [Figs. 6(f) and 7(f)]. For the same reason, we expect that the modified TFA should have a better performance in analyzing signals with linear trends or step functions.

IV. APPLICATION OF PHASE ANALYSIS TO BLOOD PRESSURE AND FLOW INTERACTION

In this section, we discuss the application of the MMPF and the TFA methods for the assessment of phase relationship between blood pressure and cerebral blood flow velocity at

the respiratory frequency (0.1–0.4Hz). To demonstrate nonstationarities and their influences, we selected three subjects including two controls (subjects 1 and 2) and one diabetic subjects (subject 3) as examples (Table I). Both blood pressure and flow signals have complex temporal structures, showing multiple oscillatory components at different time scales (Figs. 1 and 8) and different types of trends at different locations. In addition, certain artifacts during the data acquisition can also affect the signals. For examples, the BFV signal in the second subject declined abruptly at time course around 210 s and then returns to base line at 230 s [Fig. 8(b)] and the BFV signal of the third subject had a segment of missing data at ~160 s [Fig. 8(c)]. These nonstationarities introduced by intrinsic and extrinsic factors can substantially affect the estimation of BP-BFV phase relationship as we demonstrated in our simulations. For the three subjects, the estimated phase shift between blood pressure and blood flow velocity were quite different using the MMPF and using the TFA (Table I). Interestingly, the results of the modified TFA are very close to those of the MMPF (Table I). These results may be caused by the fact that nonstationarities have stronger effects on the original TFA and that the modified TFA has a better performance as we demonstrated in the simulations. The different degrees of influence on the MMPF and the TFA due to nonstationarities may also provide an explanation for the discrepancy in our previous study that the MMPF reveals a significant alteration of blood flow regulations in diabetes while the TFA could not identify the alteration using the same database (Sec. IV) [22].

V. DISCUSSSION

In this study, we systematically study the effects of different types of nonstationarities on two phase analyses. Our simulation results indicate that all tested nonstationarities have less or more influences on the performances of the TFA and the MMPF, depending on the type and the degree of nonstationarity and the frequency of interested oscillatory components. Compared to the TFA, the MMPF has generally a better performance in the presence of these nonstationarities, as evident by (i) a smaller variation in estimated phase shifts for oscillatory signals with missing data or with varying amplitude and cycle period, (ii) resistance to linear trends, and (iii) less change associated with step-function trends and with multiple oscillatory components. To minimize the effects of certain nonstationarities (e.g., trends and missing data), data preprocessing such as detrending or removing segments should be performed to obtain more reliable phase relationship. Moreover, we introduce a simple process of filtering instantaneous phase shifts in the MMPF that can automatically and efficiently eliminate the effects of missing data and step-function trends (Sec. III A and Appendix B). We also propose to apply the TFA on the interested oscillatory components extracted by the EMD or the EEMD (the modified TFA) in order to minimize the complication of multiple oscillatory components in signals (Sec. III D).

As a simulation study to test the performance of the MMPF in analyzing nonstationary signals, we only considered surrogate data with a single global linear trend or one localized step-function trend in the simulations. However, different types of nonstationarities (e.g., high-order polynomial trends, random spikes, and oscillation with nonsinusoidal wave forms) usually coexist in real data, as we demonstrated in BP and BFV signals (Sec. IV). Even for the same type of nonstationarities (e.g., linear trend), the degree of the nonstationarities (e.g., slope of linear trend) can vary at different time locations (Appendix C). All these factors will further complicate phase shift estimation. Thus, surrogate data used in our simulations were simplified cases for real-world nonstationary signals. On the other hand, this deductive approach to separate and evaluate effects of each type of nonstationarities is valuable for understanding the superposed effects of all nonstationarities in real data. In fact, these simulation results can provide more informative guidance for experimental and methodological designs to account for targeted nonstationarities, as compared to the approach of attempting to simulate superposed effects from all types of nonstationarities in a real physical or physiological signal.

In this study, we assume in our simulations that different types of nonstationarities are independent, so that their effects on results can be additive based on simulations of individual nonstationarities. However, it is possible that different nonstationarities can be inter-related and such interactions can provide important information about the underlying control mechanisms. Additionally, we consider only two oscillatory signals with a constant phase shift to simplify the simulations and interpretations. For real physical and physiological systems, phase relationship between oscillatory signals is usually not constant and often displays dynamic variations. Indeed, these variations in phase shift may provide additional information on the underlying mechanism controlling phase interactions. Therefore, further studies are needed to examine the performance of a phase analysis in estimating other variables related to dynamic phase interactions.

Nevertheless, this study provides clear evidence for three important conclusions. (1) Nonstationarity can significantly influence phase analysis and complicate the data interpretation. (2) Generally, the MMPF has a better performance than the TFA for nonstationary data. The different performance is essentially due to the different decomposition algorithm, i.e., the MMPF uses Hilbert-Huang transform while the TFA is based on Fourier transform. Therefore, one focus of future method design in phase analysis is to improve decomposition or filtering algorithm. (3) Nonstationarities in physical and physiological data are often unavoidable. However, their effects on the phase analysis can be minimized by applying concepts and strategies derived from nonlinear dynamics, mathematics, and statistical physics. As a demonstration, we proposed the modified TFA and the MMPF methods in this study and showed that they have better performances for certain specific types of nonstationarities. These findings will provide a useful guidance for further method designs aiming to better assess nonlinear interactions between nonstationary signals.

Acknowledgments

This study was supported by NIH-NINDS Grant No. R01-NS045745 to V.N., NIH-NINDS STTR Grant No. 1R41NS053128-01A2 to V.N. in collaboration with DynaDx, Inc., and General Clinical Research Center (GCRC) Grant No. MO1-RR01302. C.-K.P. gratefully acknowledges the support from the NIH/NIBIB and NIGMS (Grant No. U01-EB008577), the NIH/NIA OAIC (Grant No. P60-AG08814), the Defense Advanced Research Projects Agency (DARPA) (Grant No. HR0011-05-1-0057), the Ellison Medical Foundation, the James S. McDonnell Foundation, and the G. Harold and Leila Y. Mathers Charitable Foundation. M.-T.L. was supported by NSC (Taiwan, ROC) Grant No. 97-2627-B-008-006 and joint foundation of CGH and NCU Grant No. CNJRF-96CGH-NCU-A3. K.H. acknowledges the support from the NIH/NHLBI (Grant No. K24 HL076446) and the DOD (Grant No. PR066492).

References

1. Friesen WO, Block GD. Am J Physiol 1984;246:R847. [PubMed: 6742159]
2. Turrigiano G. Curr Opin Neurobiol 2007;17:318. [PubMed: 17451937]
3. Rosenblum MG, Pikovsky AS, Kurths J. Phys Rev Lett 1996;76:1804. [PubMed: 10060525]
4. Schafer C, Rosenblum MG, Kurths J, Abel HH. Nature (London) 1998;392:239. [PubMed: 9521318]
5. Tass P, et al. Phys Rev Lett 1998;81:3291.
6. Kantz, H.; Schreiber, T. Nonlinear Time Series Analysis. Cambridge University Press; Cambridge, England: 1997.
7. Viswanathan GM, Peng CK, Stanley HE, Goldberger AL. Phys Rev E 1997;55:845.
8. Bernaola-Galvan P, Ivanov PC, Nunes Amaral LA, Stanley HE. Phys Rev Lett 2001;87:168105. [PubMed: 11690251]
9. Huang NE, et al. Proc R Soc London, Ser A 1998;454:903.
10. Duffy DG. J Atmos Ocean Technol 2004;21:599.
11. Coughlin K, Tung KK. J Geophys Res, (Atmos) 2004;109:D21105.
12. Coughlin KT, Tung KK. Solar Variability and Climate Change 2004;34:323.
13. Tucker CJ, et al. Int J Remote Sens 2005;26:4485.

14. Yang JN, Lei Y, Lin S, Huang N. J Eng Mech 2004;130:85.
15. Yang JN, Lei Y, Pan SW, Huang N. Earthquake Eng Struct Dynam 2003;32:1533.
16. Yang JN, Lei Y, Pan SW, Huang N. Earthquake Eng Struct Dynam 2003;32:1443.
17. Huang NE, et al. Bull Seismol Soc Am 2001;91:1310.
18. Huang NE, Shen Z, Long SR. Annu Rev Fluid Mech 1999;31:417.
19. Hwang PA, Huang NE, Wang DW. Appl Ocean Res 2003;25:187.
20. Huang W, Shen Z, Huang NE, Fung YC. Proc Natl Acad Sci USA 1998;95:4816. [PubMed: 9560185]
21. Novak V, et al. Biomed Eng Online 2004;3:39. [PubMed: 15504235]
22. Hu K, et al. Physica A 2008;387:2279. [PubMed: 18432311]
23. Hu K, et al. Cardiovasc Eng 2008;8:60. [PubMed: 18080758]
24. Maestri R, et al. J Cardiovasc Electrophysiol 2007;18:425. [PubMed: 17284264]
25. Balocchi R, et al. Chaos, Solitons Fractals 2004;20:171.
26. Sweeney-Reed CM, Nasuto SJ. J Comput Neurosci 2007;23:79. [PubMed: 17273939]
27. Lo MT, et al. EURASIP J Appl Signal Process 2008;2008:785243.
28. Park J. J Sound Vibrat 2005;288:57.
29. Chen CH, Chiu HC. Soil Dyn Earthquake Eng 1998;17:371.
30. Kuo TBJ, Yang CCH, Chan SHH. Am J Physiol Heart Circ Physiol 1996;40:H2108.
31. Kuo TBJ, et al. J Cereb Blood Flow Metab 1998;18:311. [PubMed: 9498848]
32. Zhang R, Zukerman JH, Giller CA, Levine BD. Am J Physiol Heart Circ Physiol 1998;43:H233.
33. Linden D, Diehl RR, Berlit P. Electromyography and Motor Control-Electroencephalography and Clinical Neurophysiology 1998;109:387.
34. Wu Z, Huang NE. Advances in Adaptive Data Analysis 2009;1:1.
35. Xu L, et al. Phys Rev E 2006;73:065201.
36. Chen Z, et al. Phys Rev E 2006;73:031915.
37. Wu Z, Huang NE, Long SR, Peng CK. Proc Natl Acad Sci USA 2007;104:14889. [PubMed: 17846430]

Appendix

APPENDIX A: ENSEMBLE EMPIRICAL MODE DECOMPOSITION

For signals with intermittent oscillations, one essential problem of the EMD algorithm is that an intrinsic mode could comprise of oscillations with very different wavelengths at different temporal locations (i.e., mode mixing). The problem can cause certain complications for our analysis, making the results less reliable. To overcome the mode mixing problem, a noise assisted EMD algorithm, namely the EEMD, has been proposed [34]. The EEMD algorithm first generates an ensemble of data sets obtained by adding different realizations of white noise to the original data. Then, the EMD analysis is applied to these new data sets. This approach is inspired by recent study of statistical prosperities of white noise, which showed that the EMD acts as an adaptive dyadic filter bank when applied to white noise. Therefore, adding white noise would force the bits of signal with different time scales, which are automatically projected onto proper scales of reference established by the white noise. Finally, the ensemble average of the corresponding intrinsic mode functions from different decompositions or trials is calculated as the final result to cancel out the added white noise. Shortly, for a time series $x(t)$, the EEMD includes the following steps:

- **i.** Generate a new signal $y(t)$ by superposing to $x(t)$ a randomly generated white noise with amplitude equal to certain ratio of the standard deviation of $x(t)$ (applying noise with larger amplitude requires more realizations of decompositions).
- **ii.** Perform the EMD on $y(t)$ to obtain intrinsic mode functions.

iii. Iterate steps (i) and (ii) m times with different white noise to obtain an ensemble of intrinsic mode function (IMF) $\{ c_k^1(t), k=1,2\ldots n\}$, $\{ c_k^2(t), k=1,2\ldots n\}$, …, $\{ c_k^m(t), k = 1,2 \ldots n\}$.

iv. Calculate the average of intrinsic mode functions $\{ \overline{c_k(t)}, k=1,2,n\}$, where $\overline{c_k(t)}=\frac{1}{m}\sum_{i=1}^{m} c_k^i(t)$.

The last two steps are applied to reduce noise level and to ensure that the obtained IMFs reflect the true oscillations in the original time series $x(t)$. In this study, we repeat decomposition m times to make sure the noise is reduced to negligible level.

APPENDIX B: IMPROVED MMPF METHOD

To eliminate effects of nonstationarities (e.g., missing data) on the MMPF method, we modify the last step of the MMPF, in which the mean phase difference $\Delta\theta_{\mathrm{MMPF}}$ is calculated from the instantaneous phase difference $\Delta\theta(t)$ between two signals. Instead of averaging the phase difference $\Delta\theta(t)$ over all sampled points directly, we first evaluate the histogram [or probability density function, denoted as $P(\Delta\theta)$]of phase difference $\Delta\theta(t)$ and attempt to remove the contribution of missing data from the histogram. Since the values of $\Delta\theta(t)$ during the missing segments obey a uniform distribution from $-\pi$ to $-\pi$ (Sec. III A), we can estimate the uniform distribution B from the value of $P(\Delta\theta)$ at phase difference between -0.8π to -0.7π or between 0.7π and 0.8π, i.e., we assume that only missing data significantly contribute to phase shift with large magnitudes while the phase shift between real signals has relatively small values. Thus, $\Delta\theta_{\mathrm{MMPF}}$ can be calculated from the density function $P(\Delta\theta)- B$,

$$\Delta\theta_{\mathrm{MMPF}}=\int_{-\pi}^{\pi}\Delta\theta\frac{[P(\Delta\theta)-B]}{\int_{-\pi}^{\pi}[P(\Delta\theta)-B]d_{\Delta\theta}}d_{\Delta\theta}. \tag{B1}$$

As we demonstrate in Sec. III A, the modified MMPF has a better performance than the original MMPF when there are noisy or missing portions in data.

APPENDIX C: EXAMPLE OF POLYNOMIAL DETRENDING IN DIFFERENT LOCAL LINEAR TRENDS

To minimize effects of the linear trend and to obtain reliable estimate of phase shift between two oscillatory signals, a detrending process (i.e., removing polynomial trends in two signals) is usually performed before applying the TFA method [32]. A single linear trend can be removed using polynomial fitting. However, different local linear trends are usually present in a real signal. It is not a trivial task to filter such trends in the signal. Figure 9 is an example to show that such complicated trends are not easily removed by polynomial fitting. In Fig. 9, the surrogate data are composed of a pure sinusoidal oscillation and a nonstationary trend, which is constructed by cascading several linear functions with random slopes and durations one by one [see Fig. 9(b)]. Inspection of Fig. 9(d) shows that EMD can separate the sinusoidal oscillations and trends completely; however, such trends cannot be perfectly fitted by polynomial equation; thus, the residual is apparent as shown in Fig. 9(c) even utilizing the high-order polynomials. Accordingly, after polynomial detrending, the residual trend still complicates phase shift estimation.

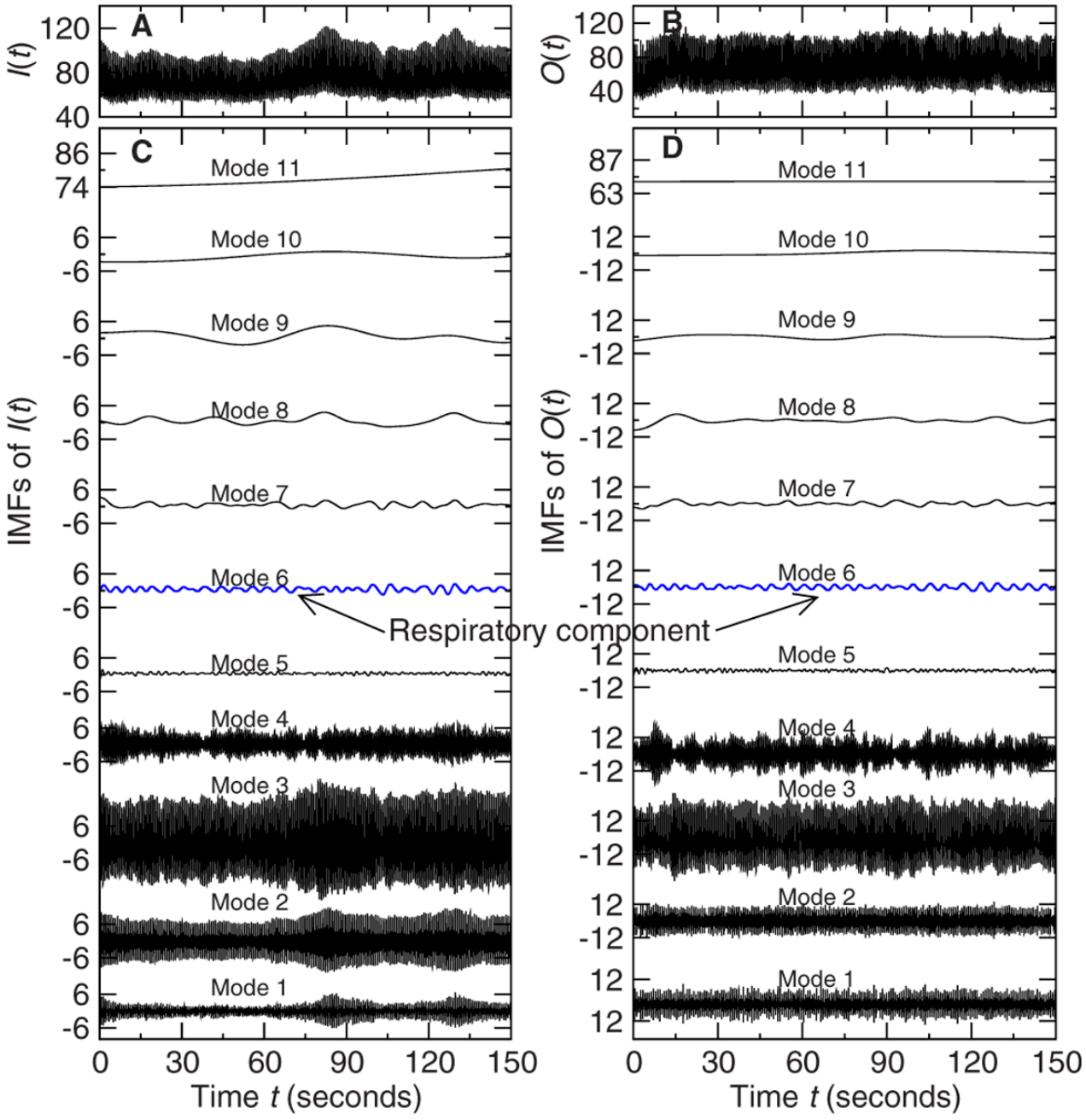

FIG. 1.

(Color online) Demonstration of empirical mode decomposition. (a) Input and (b) output signals are blood pressure and cerebral blood flow velocity of an old subject during supine rest conditions, respectively. Intrinsic mode functions (IMFs) of (c) input and (d) output signals. IMFs of mode 6 in two signals correspond to the oscillations induced by respiration.

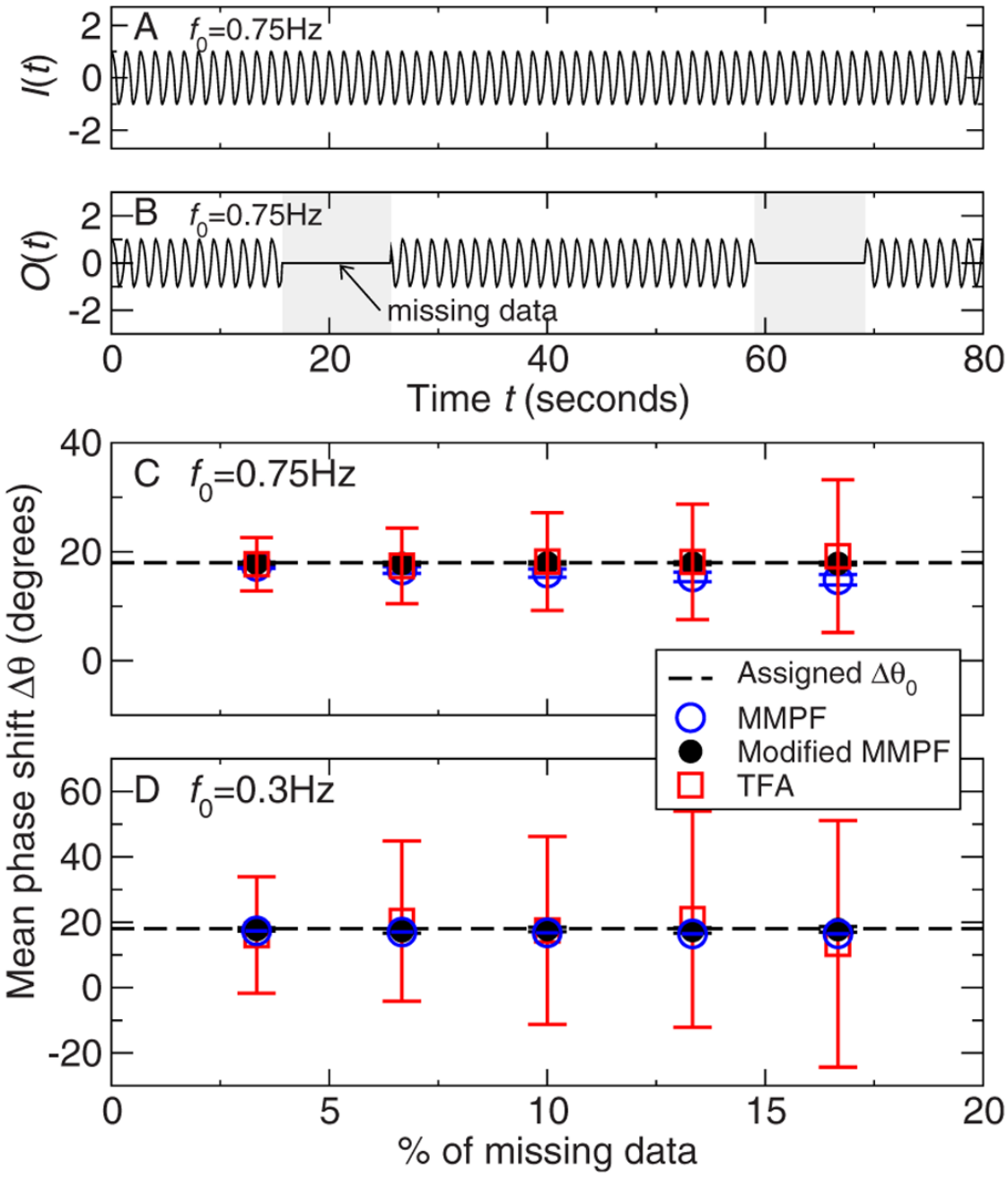

FIG. 2.

(Color online) Effect of missing data on the estimation of phase shift. (a) and (b) Examples of (a) surrogate input signal and (b) corresponding output oscillatory data with missing segments. Phase shifts between the input and the output oscillatory signals for oscillations at (c) 0.75 or (d) 0.3 Hz. Phase shifts were calculated from the MMPF, the modified MMPF, and the TFA methods. For a fixed percentage of missing data, mean, and standard deviation (error bar) of phase shifts were obtained from 50 realizations. The dashed line in (c) and (d) indicates the assigned phase shift $\Delta\theta_0$ =18°.

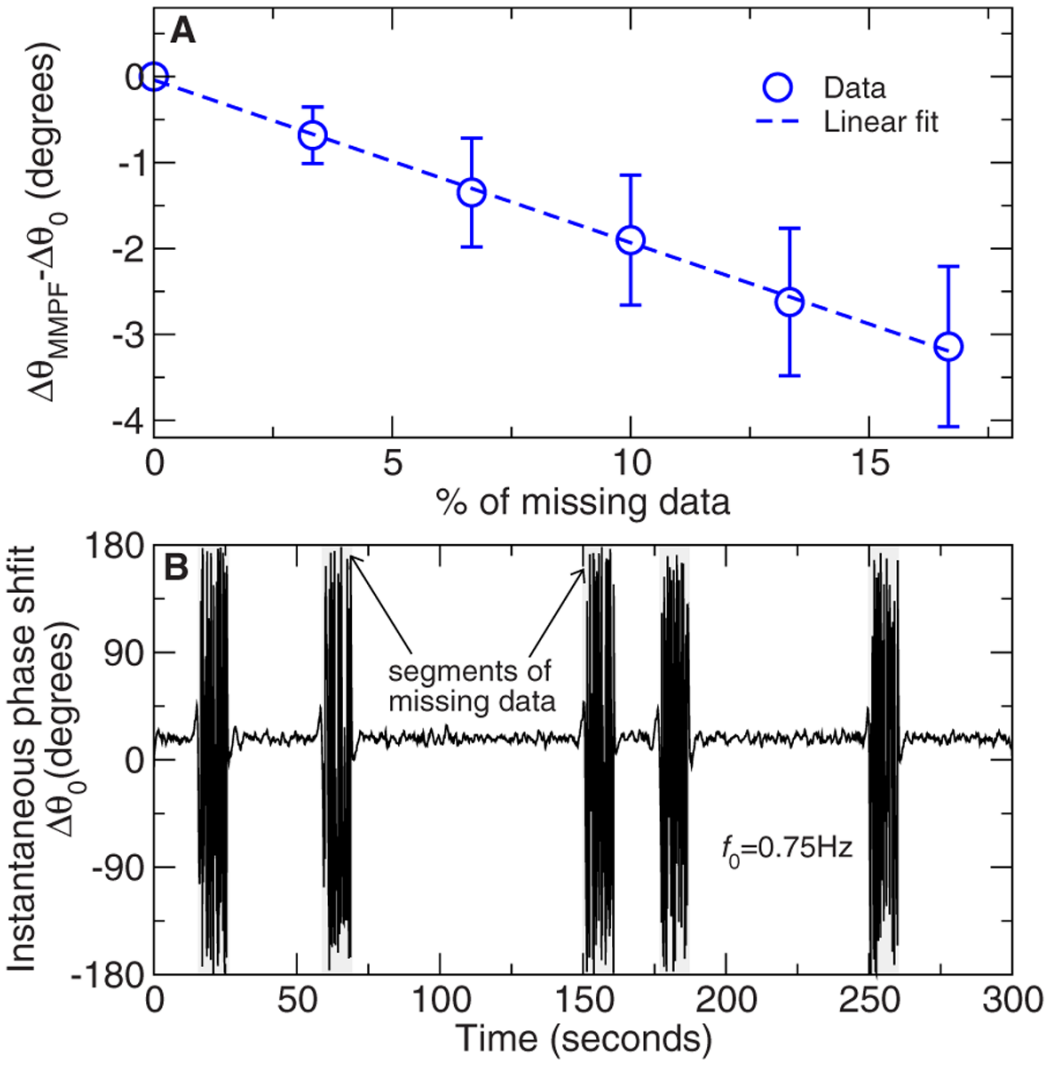

FIG. 3.

(Color online) Effects of missing data on the MMPF method. (a) The deviation of the MMPF estimated phase shift from the assigned value ($\Delta\theta_{MMPF} - \Delta\theta_0$) is linearly proportional to percentage of missing data. (b) Instantaneous phase shift $\Delta\theta_{MMPF}(t)$ obtained from the MMPF. In the segments of missing data, there is a large variation in $\Delta\theta_{MMPF}(t)$, ranging from ~−180° to ~180°.

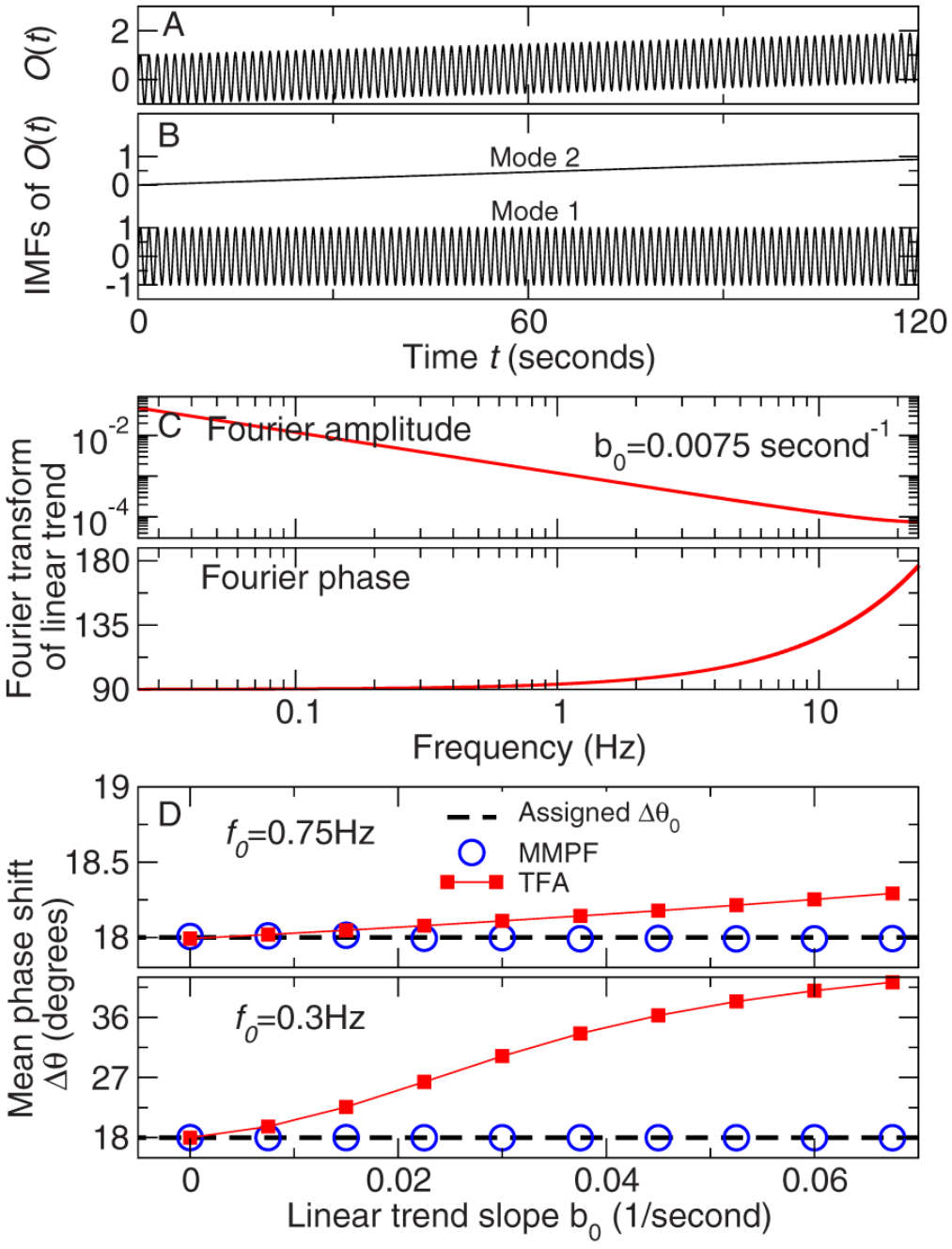

FIG. 4.

(Color online) Effect of linear trends on the estimation of phase shift. (a) Surrogate output oscillatory signal with a linear trend. The input signal is the same as shown in Fig. 3(a). (b) Decomposed IMFs of the output signal in (a). The EEMD is used for the decomposition. (c) Fourier amplitude of a linear trend. (d) Mean phase shifts between input and output signals with oscillations at high frequency (0.75 Hz) or at low frequency (0.3 Hz). Phase shifts were calculated from MMPF and TFA methods for different slopes of the linear trend in output signal.

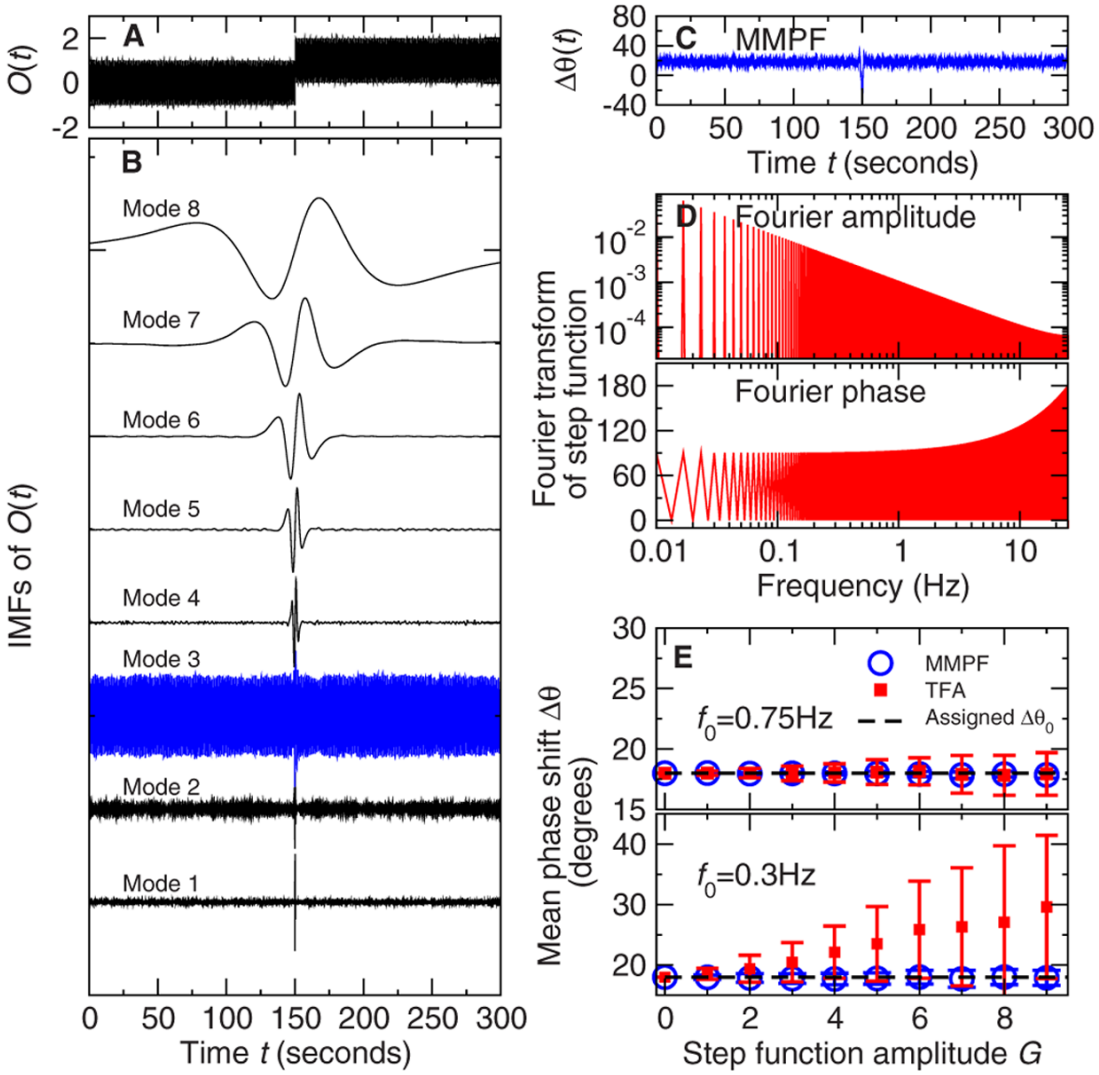

FIG. 5.

(Color online) Effect of step-function trends on the estimation of phase shift. (a) Surrogate output oscillatory signal with a step-function trend. The input signal is the same as shown in Fig. 3(a). (b) Decomposed IMFs of the output signal in (a). The EEMD is used for the decomposition. (c) Instantaneous phase shift obtained from MMPF method. (d) Fourier amplitude and phase of a step-function trend at different frequencies. (e) Mean phase shifts between input and output signals with oscillations at high (0.75 Hz) or at low (0.3 Hz) frequency. Phase shifts were calculated from MMPF and TFA methods for different amplitudes of the step-function trend in output signal. For each amplitude of step-function trend, mean and standard deviation (error bar) of phase shifts were obtained from 50 realizations. In each realization, the location of jump, t_1, was randomly chosen from a uniform distribution (0–300 s).

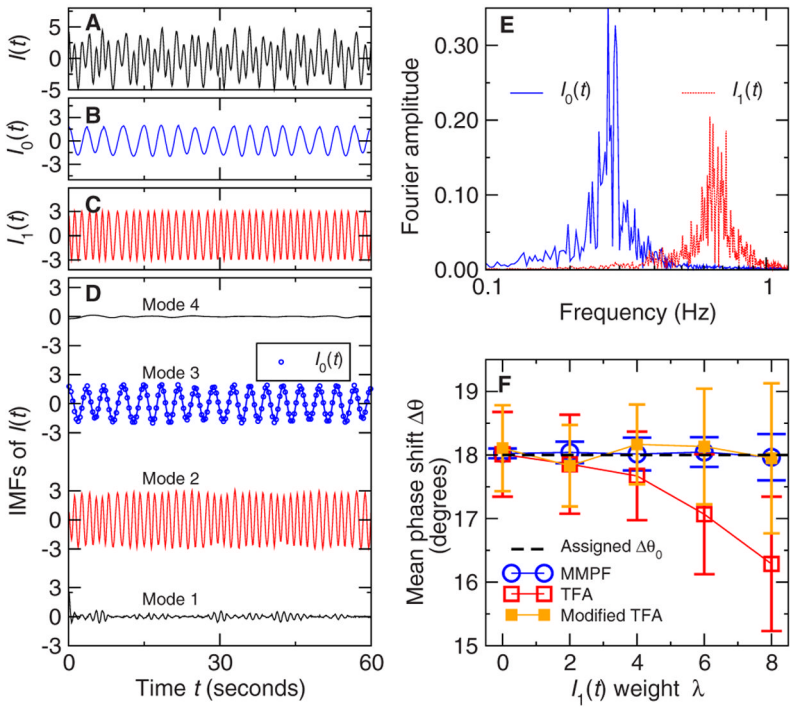

FIG. 6.

(Color online) Effect on the phase shift estimation of two oscillatory components without significant overlapping in frequent domain. (a) A surrogate input signal $I(t)$ with two oscillatory components. (b) $I_0(t)$ at low frequency (centered at 0.28 Hz) and (c) $I_1(t)$ at high frequency (centered at 0.7 Hz). Both components have varying amplitudes and cycle periods that obey uniform distributions. (d) IMFs of the input signal $I(t)$ obtained from the EEMD. Mode 3 IMF represents closely the component $I_0(t)$ in (b) and mode 2 IMF represents the component $I_1(t)$ in (c). (e) Fourier amplitude of $I_0(t)$ and $I_1(t)$ at different frequencies. (f)Phase shifts calculated from the MMPF, the TFA, and the modified TFA methods for different weights of $I_1(t)$ in the input signal [$I(t) = I_0(t) + \lambda I_1(t)$]. Data are presented as mean and standard deviation (error bar). Each data point was from 50 realizations.

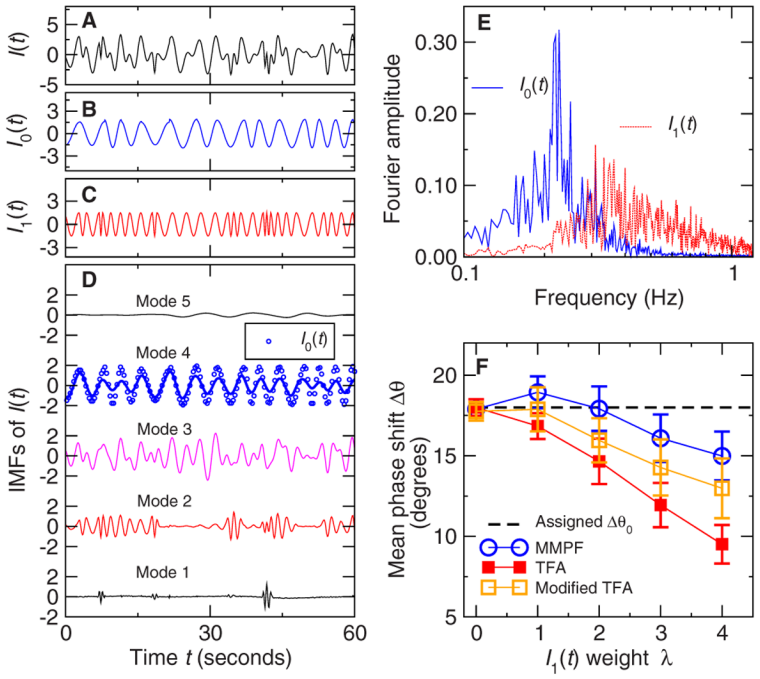

FIG. 7.

(Color online) Effect on the phase shift estimation of two oscillatory components with a significant overlap in frequent domain. (a) A surrogate input signal $I(t)$ with two oscillatory components: (b) $I_0(t)$ at low frequency (centered at ~0.25 Hz) and (c) $I_1(t)$ at high frequency (centered at ~0.4 Hz). Both components have varying amplitudes and cycle periods that obey a uniform distribution. (d) IMFs of the input signal $I(t)$ obtained from the EEMD. Mode 4 IMF represents mostly the component $I_0(t)$ in (b), mode 2 IMF represents partially the component $I_1(t)$ in (c), and mode 3 is contributed partially by $I_0(t)$ and partially by $I_1(t)$. (e) Fourier amplitudes of $I_0(t)$ and $I_1(t)$ at different frequencies show a significant overlap between the components of $I_0(t)$ and $I_1(t)$ in frequency domain. (f) Mean phase shifts calculated from the MMPF, the TFA, and the modified TFA methods for different weights of $I_1(t)$ in the input signal $[I(t) = I_0(t) + \lambda I_1(t)]$. Data are presented as mean and standard deviation (error bar). Each data point was from 50 realizations.

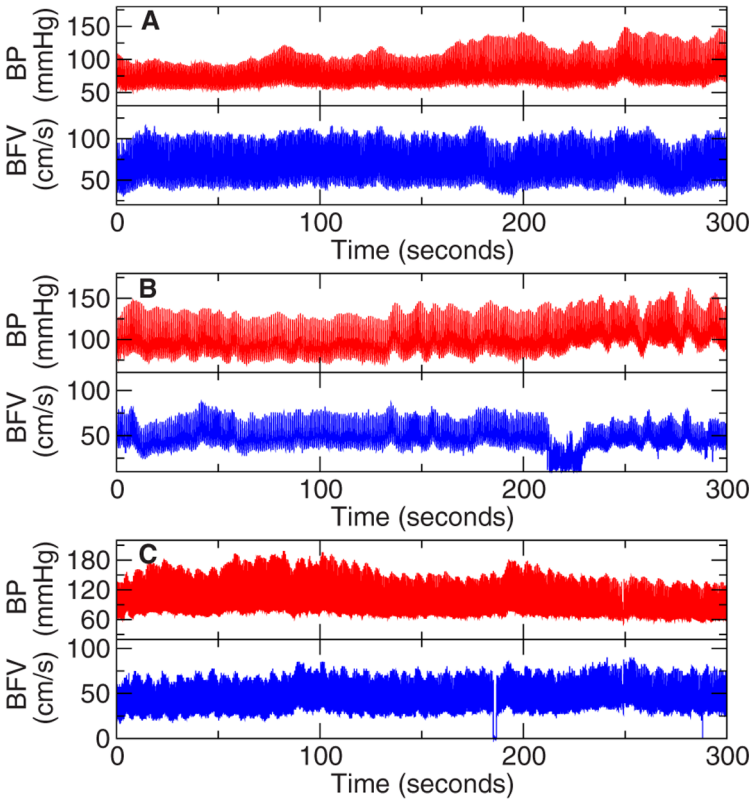

FIG. 8.

(Color online) Different types of nonstationarities in blood pressure (BP) and cerebral blood flow velocity (BFV). (a) The same BP and BFV signals in healthy elderly subject as shown in Fig. 1. There are intrinsic multiple oscillatory components that correspond to different physiological processes (Fig. 1). (b) BP and BFV signals in a healthy elderly subject. There is a segment of BFV (210–230 s) with a bad quality that might be caused by external influences during the data acquisition. (c) BP and BFV signals in a patient with diabetes. BFV drops to zero at two locations due to interruptions during the recording.

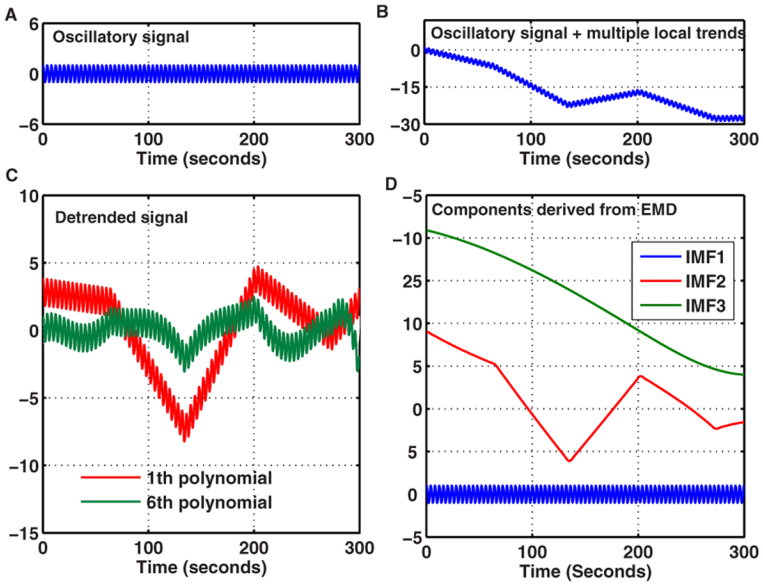

FIG. 9.

(Color online) (a) A surrogate oscillatory signal. (b) The signal in (a) superposed with multiple local linear trends. (c) Extracted oscillatory signal by linear detrending and sixth-order polynomial detrending. (d) Decompositions of surrogate data by EMD.

TABLE I

MMPF, TFA, and modified TFA results of phase shifts between blood pressure and blood flow velocity in three representative subjects.

Subject	Phase shift (deg)		
	MMPF	TFA	Modified TFA
1	31.1	15.5	26.1
2	36.5	18.0	39.5
3	13.1	27.3	13.9